Influence of Annealing Conditions on Magnetic Properties, Magnetocaloric Effect, and Critical Parameters of Ni–Mn–Sn Ribbons

Nguyen Hai Yen[1, 2], Pham Thi Thanh[1, 2], Victor V. Koledov[3], Alexander P. Kamantsev[3], Alexey V. Mashirov[3], Tran Dang Thanh[1, 4], Kieu Xuan Hau[1, 4], Seong Cho Yu[4], and Nguyen Huy Dan[1, 2]

[1]Institute of Materials Science, Vietnam Academy of Science and Technology, 18 Hoang Quoc Viet, Hanoi 100000, Vietnam
[2]Graduate University of Science and Technology, Vietnam Academy of Science and Technology, 18 Hoang Quoc Viet, Hanoi 100000, Vietnam
[3]Laboratory of Magnetic Phenomena in Microelectronics, Kotelnikov Institute of Radioengineering and Electronics of RAS, 125009 Moscow, Russia
[4]Department of Physics, Chungbuk National University, Cheongju 361-763, South Korea

In this paper, we investigated the influence of annealing conditions on magnetic properties, magnetocaloric effect, and critical parameters of $Ni_{50}Mn_{50-x}Sn_x$ ($x = 13$, 13.5, and 14) alloy ribbons prepared by using the melt-spinning method. The ribbons were annealed at 1123 K for various times. A martensitic–austenitic (M–A) structural phase transformation was observed on both the as-quenched and annealed samples. Temperature of the M–A phase transition (T_{M-A}) of the ribbons can be regulated in room temperature region by changing the annealing time. Maximum positive and negative magnetic entropy changes, $|\Delta S_m|_{max}$, larger than 3 and 1 $J \cdot kg^{-1} \cdot K^{-1}$, respectively, were achieved on the $Ni_{50}Mn_{37}Sn_{13}$ sample after annealing for 0.5 h. Critical parameters were determined to elucidate magnetic orders in the alloy. The obtained parameters are very close to those of the mean field theory of long-range ferromagnetic orders.

***Index Terms*— Heusler alloy, magnetic entropy change, magnetocaloric effect (MCE), melt-spinning method, phase transition temperature.**

I. Introduction

MAGNETOCALORIC effect (MCE) is defined as the adiabatic change of temperature of a magnetic material (heated or cooled) when it is magnetized or demagnetized. The MCE of a material can be assessed through its magnetic entropy change (ΔS_m), the adiabatic temperature change (ΔT_{ad}), and the refrigerant capacity (*RC*). Practically, this effect was discovered a long time ago, basing on the temperature change of iron in variation of applied magnetic field. The first application of MCE was the use of paramagnetic $Gd_2(SO_4)_3.8H_2O$ salts to achieve the low temperature, less than 1 K [1], [2]. Especially, in 1997, the achievement of the giant MCE (GMCE) in Gd–Si–Ge alloys around 300 K manifested application potential of magnetic refrigeration technology at room temperature [3]. Therefore, the search for materials with GMCE in room temperature region has been attracting many scientists. Up to now, a number of magnetic materials possessing GMCE have been discovered, such as Gd-containing alloys, As-containing alloys, La-containing alloys, Heusler alloys, Fe- and Mn-based rapidly quenched alloys, and ferromagnetic perovskite manganites [4].

Among the abovementioned magnetocaloric materials, Ni–Mn–Z (Z = Ga, In, Sn, ...) Heusler alloys have considerably concentrated to study. These alloys have both the first-order phase transition (FOPT) and second-order phase transition (SOPT) [5]–[8]. The reason for having the FOPT is the martensitic–austenitic (M–A) structural phase transformation. Both the magnetic phase transition types in Heusler alloys can cause GMCE. The positive GMCE relates to the SOPT, and negative GMCE corresponds to the FOPT. Ni–Mn–Sn alloy is a typical one. Negative GMCE of this system was reported by Krenke *et al.* [6] in the Nature Materials. According to Krenke *et al.* [6], the maximum magnetic entropy change, $|\Delta S_m|_{max}$, of the Ni–Mn–Sn alloy is about 18 $J \cdot kg^{-1} \cdot K^{-1}$ under the magnetic field change of 50 kOe at room temperature. However, structural and magnetic properties of the alloy are so sensitive with composition and fabrication condition. The previous studies often focused on the bulk form of the alloy. The bulk alloys commonly required complex thermal treatment and long annealing time (up to several days). Recently, some reports showed that by using the melt-spinning method, one can create relative single phase, shorten annealing time, and improve MCE for the Heusler alloys [5], [7], [9]. In this paper, we studied the influence of annealing conditions on magnetic properties, MCE, and critical parameters of $Ni_{50}Mn_{37-x}Sn_x$ ($x = 13$, 13.5, and 14) alloy ribbons.

II. Experiment

Ingots with nominal compositions of $Ni_{50}Mn_{50-x}Sn_x$ ($x = 13$, 13.5, and 14) were prepared from pure components of Ni, Mn, and Sn on an arc-melting furnace to ensure their homogeneity. The ribbons were then fabricated from the ingots on a single wheel melt-spinning system. The quenching

Manuscript received December 5, 2017; revised March 8, 2018 and March 9, 2018; accepted March 13, 2018. Corresponding author: N. H. Yen (e-mail: yennh@ims.vast.ac.vn).

Color versions of one or more of the figures in this paper are available online at http://ieeexplore.ieee.org.

Digital Object Identifier 10.1109/TMAG.2018.2816952

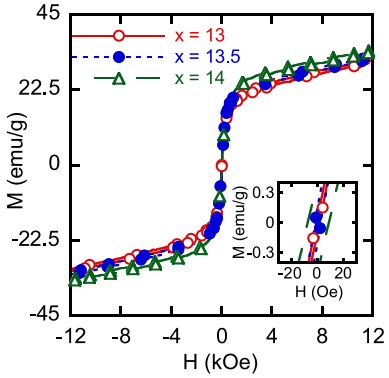

Fig. 1. Hysteresis loops at room temperature of as-quenched $Ni_{50}Mn_{37-x}Sn_x$ ($x = 13$, 13.5, and 14) ribbons.

rate of the ribbons could be changed by changing tangential velocity v of the copper wheel. In this paper, the ribbons were prepared with $v = 40$ m/s. Subsequently, the ribbons were annealed at 1123 K for various times. All of the arc-melting, melt-spinning, and annealing processes were performed under Ar atmosphere to avoid oxygenation. Structural analyses of the as-quenched ribbons were performed at room temperature by using an X-ray diffraction in the range of 20°–70°. Magnetization measurements in the temperature range of 77–400 K were performed on a vibrating sample magnetometer. Magnetic entropy change ΔS_m of these alloy ribbons was calculated via

$$\Delta S_m = -\int_0^H \left(\frac{\partial M}{\partial T}\right) \mathrm{dH}. \quad (1)$$

III. Results and Discussion

Thickness of the obtained ribbons is about 30 μm. The XRD results show that the as-quenched ribbons exhibit single phase with an austenitic L21-cubic structure, which belongs to the space group Fm3m [10]. This is in good agreement with other studies. The M–A phase transition in the as-quenched Ni–Mn–Sn ribbons occurs below room temperature [11], [12].

Magnetic properties of the alloy ribbons were characterized by magnetization measurements in varying magnetic field and temperature. Fig. 1 shows hysteresis loops of the as-quenched $Ni_{50}Mn_{50-x}Sn_x$ ($x = 13$, 13.5, and 14) alloy ribbons at room temperature. We can see that all the ribbons are soft magnetic with coercivity less than 30 Oe (see the inset of Fig. 1). This is good for magnetic refrigeration because the magnetic hysteresis loss should be very small or negligible. Besides, the saturation magnetization of the as-quenched alloy ribbons was slightly increased with increasing Sn concentration. This can be due to the change of the exchange interactions of the atoms in the alloy when the Sn concentration is changed. According to [13] and [14], the Mn atoms could be coupled ferromagnetically or antiferromagnetically depending on composition of the alloys. The various exchange interactions could make the alloys become weak or strong ferromagnets with different saturation magnetizations and Curie temperatures.

Fig. 2 presents thermomagnetization curves in an applied magnetic field of 12 kOe of the as-quenched and annealed

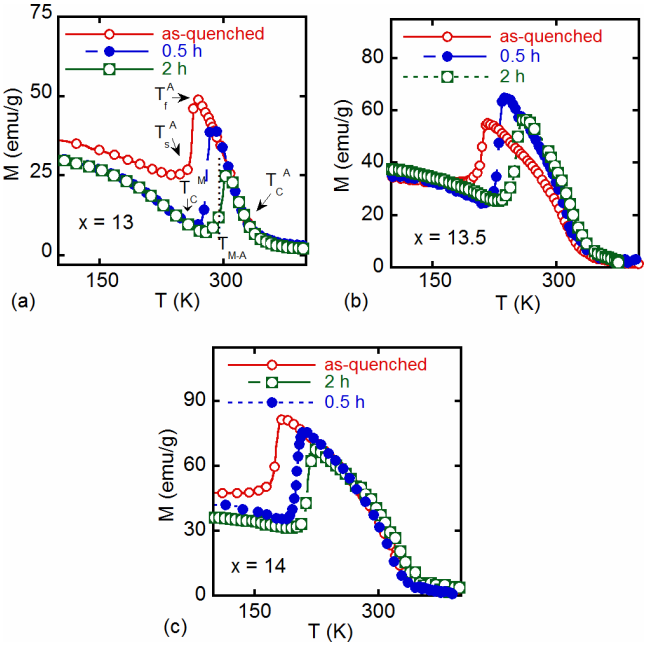

Fig. 2. Thermomagnetization curves in an applied field of 12 kOe of $Ni_{50}Mn_{50-x}Sn_x$ ribbons with (a) $x = 13$, (b) $x = 13.5$, and (c) $x = 14$ before and after annealing at 1123 K for various times.

$Ni_{50}Mn_{50-x}Sn_x$ alloy ribbons with various Sn concentrations. The obtained results show that both the martensitic and austenitic phases occur in all the samples. The martensitic phase relates to weak ferromagnetic or antiferromagnetic orders, while the austenitic phase is strong ferromagnetic [14], [15]. In general, by heating up the Ni–Mn–Sn alloy ribbons from low temperature, the magnetization decreases to a minimum at the transition temperature of the martensitic phase (T_C^M) then fast increases at the austenitic start temperature (T_s^A). The increase of magnetization stops at the austenitic finish temperature (T_f^A). The last magnetic transition of the ferromagnetic-to-paramagnetic (FM–PM) phase occurs at the Curie temperature of the austenitic phase (T_C^A). It should be noted that the range of Sn concentration for the existence of the martensite in the alloys is rather narrow (in few percent) and the volume fract ion of the martensite strongly depends on the fabrication conditions [16]. The M–A phase transition temperature (T_{M-A}) and magnitude of the FOPT strongly depend on the Sn concentration and annealing process. The T_{M-A} of the as-quenched alloy fast decreases from 255 (for $x = 13$) to 182 K (for $x = 14$), while the Curie temperature T_C^A slightly increases with increasing Sn concentration. Besides, we also see that the T_{M-A} of the ribbons can be regulated in room temperature region by changing the annealing time. Specially, after annealing at 1123 K for 2 h, the T_{M-A} of the sample with $x = 13$ is raised to ~300 K. However, the T_C^A is almost unchanged by this annealing process. Thus, the effect of the Sn concentration and annealing process on the FOPT has a significant meaning in controlling the working temperature of the magnetic refrigerants.

Among these samples, we can see that the $Ni_{50}Mn_{37}Sn_{13}$ ribbon samples, after annealing for 0.5 and 2 h, show two strong magnetic phase transitions near room temperature.

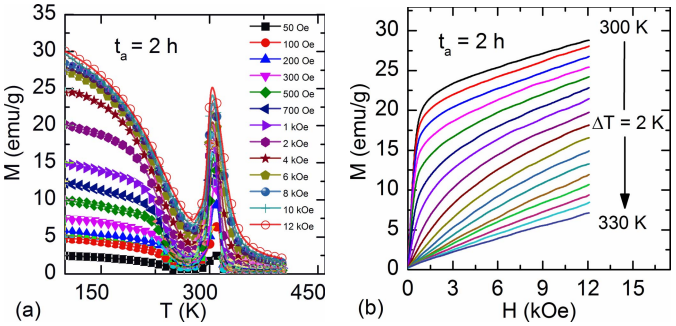

Fig. 3. Thermomagnetization curves in (a) various magnetic fields and (b) magnetization versus magnetic field at different temperatures of $Ni_{50}Mn_{37}Sn_{13}$ alloy ribbons after annealing at 1123 K for 2 h.

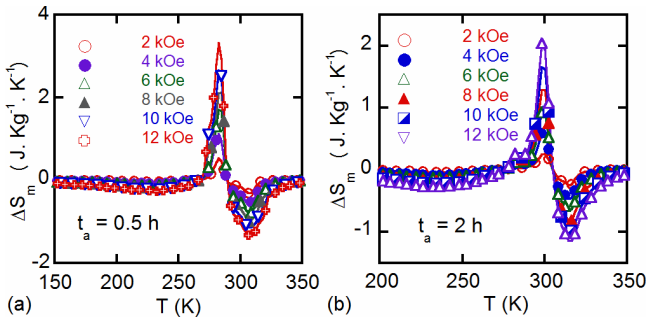

Fig. 4. $\Delta S_{\rm m}(T)$ curves ($\Delta H = 12$ kOe) of $Ni_{50}Mn_{37}Sn_{13}$ ribbons after annealing at 1123 K for (a) 0.5 and (b) 2 h.

Therefore, we chose these samples to investigate their MCE. Fig. 3(a) shows thermomagnetization curves in magnetic field ranging from 0.05 to 12 kOe of the $Ni_{50}Mn_{37}Sn_{13}$ alloy ribbons after annealing at 1123 K for 2 h. The magnetization of the sample increases with magnetic field. Besides, we can see that all the thermomagnetization curves have phase transition temperatures around 300 K.

The MCE of the alloy was assessed by the magnetic entropy change ($\Delta S_{\rm m}$). In order to calculate the magnetic entropy change of the alloy ribbons, the series of $M(H)$ curves were determined at various temperatures around the FOPT and SOPT [Fig 3(b)]. The $\Delta S_{\rm m}$ for the alloys was calculated by using the relation (1).

Fig. 4 shows temperature dependence of $\Delta S_{\rm m}$ of the $Ni_{50}Mn_{37}Sn_{13}$ ribbons with annealing process at 1123 K for 0.5 and 2 h under several magnetic field changes ($\Delta H = 2$, 4, 6, 8, 10, and 12 kOe). It can be observed that both the negative and positive MCEs coexist in the samples. The positive MCE ($\Delta S_{\rm m} < 0$) is due to the second-order FM–PM phase transition. The negative MCE ($\Delta S_{\rm m} > 0$) is related to the first-order M–A phase transition. The $\Delta S_{\rm m}$ value increases with increasing the magnetic field. For $\Delta H = 12$ kOe, the maximum magnetic entropy changes, $|\Delta S_{\rm m}|_{\rm max}$, of the negative MCE are 3.3 and 2.2 $\rm J \cdot kg^{-1} \cdot K^{-1}$ around $T_{M-A} = 283$ and 300 K for the samples after annealing for 0.5 and 2 h, respectively. These values are higher than those obtained for other Heusler alloys such as $Ni_{50}Mn_{37}Sn_{13}$ ingot [16], $Ni_{40-x}Co_xMn_{50}Sn_{10}$ alloys [17], $Ni_{50}Mn_{35.8}Sn_{14.2}$ ribbons [18], and $Ni_{50-x}Ag_xMn_{37}Sn_{13}$ ribbons [19]. However, these values are only retained in a narrow temperature range

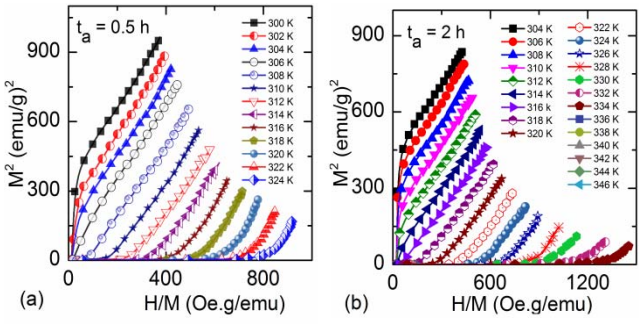

Fig. 5. M^2–H/M plots at different temperatures of $Ni_{50}Mn_{37}Sn_{13}$ ribbons after annealing at 1123 K for (a) 0.5 h and (b) 2 h.

due to the nature of the FOPT. The full width at half maximum of entropy change peak ($\delta T_{\rm FWHM}$) around T_{M-A} is about 10 K two times larger than that of the as-quenched ribbon sample [10].

For the case of positive MCEs, $|\Delta S_{\rm m}|_{\rm max}$ is 1.3 and 1.1 $\rm J \cdot kg^{-1} \cdot K^{-1}$ (with $\Delta H = 12$ kOe) around $T_C^A = 308$ and 316 K for the samples after annealing for 0.5 and 2 h, respectively. These values are smaller than those of the negative MCEs. However, the $\Delta S_{\rm m}(T)$ curves around T_C^A are distributed over a wide temperature range due to the nature of the SOPT. In addition, both the samples also exhibited an extreme with $|\Delta S_{\rm m}|_{\rm max} \approx 0.3 \rm J \cdot kg^{-1} \cdot K^{-1}$ for $\Delta H = 12$ kOe around 250 K, which can be attributed to magnetic transitions at the Curie temperature of the martensitic phase.

It should be noted that the maximum magnetic entropy change of the ribbons can be regulated in room temperature region by appropriate annealing processes. After annealing, the maximum positive magnetic entropy change of $Ni_{50}Mn_{37}Sn_{13}$ ribbons is shifted from 255 K (the as-quenched sample) to ~300 K (the sample annealed at 1123 K for 2 h). Thus, both the positive and negative MCEs of the ribbons are close to room temperature. Therefore, it is possible for combining all the positive and negative MCEs of the $Ni_{50}Mn_{37}Sn_{13}$ ribbons for magnetic refrigeration application at room temperature.

In order to understand the nature of the magnetic interactions in the alloys, we investigated their critical behavior around T_C^A by using Arrott plots [20]. The Arrott plots, M^2 versus H/M (Fig. 5), around T_C^A were plotted from $M(H)$ data. Because the FM–PM transition is continuous, the spontaneous magnetization (M_s) and the inverse initial susceptibility (χ_0^{-1}) at different temperatures could be derived from Arrott plots. The critical parameters of β, γ, and T_C relate to the two above quantities by the following equations:

$$\rm M_s(T) = M_0(-\varepsilon)^{\beta} \varepsilon < 0 \tag{2}$$

$$\chi_0^{-1}(T) = \frac{\rm H_0}{\rm M_0}\varepsilon^{\gamma}\ \varepsilon > 0 \tag{3}$$

where $\rm M_0$ and $\rm H_0$ are the critical amplitudes and $\varepsilon = (T - T_C^A)/T_C^A$ is the reduced temperature.

δ can be calculated by using the Widom scaling relation [21]

$$\delta = 1 + \gamma/\beta. \tag{4}$$

The linear extrapolations from high magnetic field region to the intercepts with the M^2 and H/M axes give the values

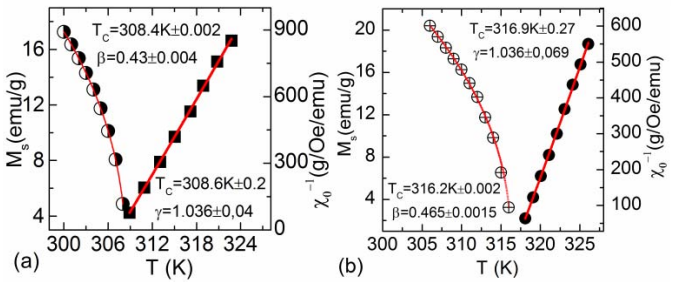

Fig. 6. Temperature dependence of spontaneous magnetization $M_s(T)$ and inverse initial susceptibility $\chi_0^{-1}(T)$ of the $Ni_{50}Mn_{37}Sn_{13}$ ribbons after annealing at 1123 K for (a) 0.5 h and (b) 2 h.

of $M_s(T)$ and $\chi_0^{-1}(T)$, respectively. The T_C, β, and γ were obtained from fitting $M_s(T)$ and $\chi_0^{-1}(T)$ data (Fig. 6) by using (2) and (3). Meanwhile, δ can be calculated by (4). As resulted, the ribbons with annealing time for 0.5 h have the critical parameters of $\beta \approx 0.43$, $\gamma \approx 1.036$, $\delta \approx 3.37$, and $T_C \approx 308$ K. Similarly, for the sample with annealing time of 2 h, those values are $\beta \approx 0.465$, $\gamma \approx 1.021$, $\delta \approx 3.23$, and $T_C \approx 316$ K. One can realize that the T_C of the alloy ribbons obtained from the fittings is mostly equal to that directly determined from the thermomagnetization measurements. This means that the procedures of deducing and fitting data are corrected. In comparison with some standard models such as mean field theory ($\beta = 0.5$, $\gamma = 1$, and $\delta = 3$), 3-D Heisenberg model ($\beta = 0.365$, $\gamma = 1.336$, and $\delta = 4.8$), and 3-D Ising model ($\beta = 0.325$, $\gamma = 1.241$, and $\delta = 4.82$) [22], our critical parameters obtained in this method fall between those of the mean field and 3-D Heisenberg models. The critical parameters of the ribbons with annealing time of 2 h are closer to those of the mean field theory of long-range ferromagnetic orders. This means that these samples mainly have long-range ferromagnetic orders. According to [12], the as-quenched $Ni_{50}Mn_{37}Sn_{13}$ ribbons display short-range FM orders with $\beta = 0.385$ and $\gamma = 1.083$. Thus, the annealing process plays an importance role in establishing long-range FM orders in $Ni_{50}Mn_{37}Sn_{13}$ ribbons. After annealing, the austenitic phase in these ribbons becomes more magnetically homogeneous.

IV. Conclusion

Influence of annealing process on magnetic properties, MCE, and critical parameters of $Ni_{50}Mn_{37-x}Sn_x$ ($x = 13$, 13.5, and 14) rapidly quenched ribbons was investigated. The M–A phase transition temperature T_{M-A} of the ribbons can be regulated in room temperature region by appropriate annealing time. After annealing at 1123 K for 2 h, the T_{M-A} of the sample with $x = 13$ is raised to ~300 K. The achieved maximum magnetic entropy change, $|\Delta S_m|_{max}$, of the annealed $Ni_{50}Mn_{37}Sn_{13}$ alloy ribbons associated with negative MCE is 3.3 $J \cdot kg^{-1} \cdot K^{-1}$ (with $\Delta H = 12$ kOe) at $T_{M-A} \approx 300$ K. Critical parameters of the annealed ribbons are close to those of the mean-field model for long-range ferromagnetic orders.

Acknowledgment

This work was supported in part by the Vietnam Academy of Science and Technology under Grant VAST.HTQT.NGA.05/17-18, in part by the Scientific Research and Technology Development Project for Young Researchers (2018), in part by the Russian Foundation for Basic Research under Grant 17-58-540002, in part by the Key Laboratory for Electronic Materials and Devices, Institute of Materials Science, Hanoi, Vietnam, and in part by the Laboratory of Magnetism and Superconductivity, Institute of Materials Science.

References

[1] W. F. Giauque and D. P. MacDougall, "Attainment of temperatures below 1° absolute by demagnetization of $Gd_2(SO_4)_{3.8}H_2O$," *Phys. Rev.*, vol. 43, no. 9, p. 768, Jan. 1933.
[2] F. Bitter, "Magnetization and the magneto-caloric effect," *Phys. Rev.*, vol. 38, no. 3, pp. 528–548, Aug. 1931.
[3] V. K. Pecharsky and K. A. Gschneidner, Jr, "Magnetocaloric effect and magnetic refrigeration," *J. Magn. Magn. Mater.*, vol. 200, nos. 1–3, pp. 44–56, Oct. 1999.
[4] V. Franco, J. S. Blázquez, B. Ingale, and A. Conde, "The magnetocaloric effect and magnetic refrigeration near room temperature: Materials and models," *Annu. Rev. Mater. Sci.*, vol. 42, pp. 305–342, May 2012.
[5] C. O. Aguilar-Ortiz *et al.*, "Influence of Fe doping and magnetic field on martensitic transition in Ni–Mn–Sn melt-spun ribbons," *Acta Mater.*, vol. 107, pp. 9–16, Apr. 2016.
[6] T. Krenke *et al.*, "Inverse magnetocaloric effect in ferromagnetic Ni–Mn–Sn alloys," *Nature Mater.*, vol. 4, pp. 450–454, May 2005.
[7] S. C. Ma *et al.*, "Wheel speed-dependent martensitic transformation and magnetocaloric effect in Ni–Co–Mn–Sn ferromagnetic shape memory alloy ribbons," *Acta Mater.*, vol. 90, pp. 292–302, May 2015.
[8] S. Pandey *et al.*, "Magnetic, thermal and magnetocaloric properties of $Ni_{50}Mn_{35}In_{14.5}B_{0.5}$ ribbons," *Adv. Mater. Lett.*, vol. 8, pp. 768–772, Jul. 2017.
[9] Y. Zhang *et al.*, "Enhanced magnetic refrigeration properties in Mn-rich Ni-Mn-Sn ribbons by optimal annealing," *Sci. Rep.*, vol. 5, pp. 11010-1–11010-11, Jun. 2015.
[10] H. D. Nguyen *et al.*, "Influence of fabrication conditions on giant magnetocaloric effect of Ni–Mn–Sn ribbons," *Adv. Natural Sci., Nanosci. Nanotechnol.*, vol. 4, no. 2, pp. 025011-1–025011-4, Apr. 2013.
[11] Y. B. Yang *et al.*, "Structure and exchange bias of $Ni_{50}Mn_{37}Sn_{13}$ ribbons," *J. Appl. Phys.*, vol. 111, no. 7, pp. 07A916-1–07A916-3, Feb. 2012.
[12] T.-L. Phan *et al.*, "Coexistence of conventional and inverse magnetocaloric effects and critical behaviors in $Ni_{50}Mn_{50-x}Sn_x$ (x = 13 and 14) alloy ribbons," *Appl. Phys. Lett.*, vol. 101, no. 21, pp. 212403-1–212403-5, Nov. 2012.
[13] R. Y. Umetsu *et al.*, "The effect of Co substitution on the magnetic properties of the Heusler alloy $Ni_{50}Mn_{33}Sn_{17}$," *Appl. Phys. Lett.*, vol. 98, no. 4, pp. 042507-1–042507-3, Jan. 2011.
[14] R. Y. Umetsu, A. Fujita, W. Ito, T. Kanomata, and R. Kainuma, "Determination of the magnetic ground state in the martensite phase of Ni–Mn–Z (Z = In, Sn and Sb) off-stoichiometric Heusler alloys by nonlinear AC susceptibility," *J. Phys. Condens. Matter*, vol. 23, no. 32, pp. 326001-1–326001-6, Jul. 2011.
[15] Z. Zhong, S. Ma, D. Wang, and Y. Du, "A review on the regulation of magnetic transitions and the related magnetocaloric properties in Ni-Mn-Co-Sn Alloys," *J. Mater. Sci. Technol.*, vol. 28, no. 3, pp. 193–199, Mar. 2012.
[16] N. H. Dan *et al.*, "Magnetic properties and magnetocaloric effect in Ni–Mn–Sn alloys," *J. Magn. Magn. Mater.*, vol. 374, pp. 372–375, Jan. 2015.
[17] J. Sharma and K. G. Suresh, "Investigation of multifunctional properties of $Mn_{50}Ni_{40-x}Co_xSn_{10}$ (x = 0–6) Heusler alloys," *J. Alloys Comp.*, vol. 620, pp. 329–336, Jan. 2015.
[18] A. Biswas *et al.*, "Impacts of first-order phase transition and phase coexistence on the universal behavior of inverse magnetocaloric effect," *J. Appl. Phys.*, vol. 115, no. 17, pp. 17A907-1–17A907-3, Jan. 2014.
[19] T. D. Thanh *et al.*, "Magnetic and magnetocaloric properties of Ni-Ag-Mn-Sn ribbons and their composites," *J. Alloys Comp.*, vol. 696, pp. 1129–1138, Mar. 2017.
[20] A. Arrott and J. E. Noakes, "Approximate equation of state for nickel near its critical temperature," *Phys. Rev. Lett.*, vol. 19, pp. 786–789, Oct. 1967.
[21] B. Widom, "Degree of the critical isotherm," *J. Chem. Phys.*, vol. 41, no. 6, pp. 1633–1634, 1964.
[22] H. E. Stanley, *Introduction to Phase Transitions and Critical Phenomena*, Oxford, U.K.: Oxford Univ. Press, 1971.